JOURNAL OF MATERIALS SCIENCE 22 (1987) 629–637

Phase formation in co-deposited metallic alloy thin films

N. SAUNDERS, A. P. MIODOWNIK
Department of Materials Science and Engineering, University of Surrey, Guildford, Surrey GU2 5XH, UK

Phase formation in co-deposited thin films of Pd–Rh, Cu–Ag and Cu–Sn has been examined. Depending on the substrate temperature, either equilibrium or non-equilibrium phases are formed. It is postulated that the formation of multiphase structures in co-deposited alloy thin films is controlled by the diffusional breakdown of fully intermixed depositing atoms, so that three kinetic regimes are observed: (i) at low substrate temperatures the surface mobility is insufficient for the decomposition of the fully intermixed depositing atoms and the films contain non-equilibrium single-phase structures; (ii) with increasing substrate temperature decomposition to non-equilibrium two phase structures is observed; and finally (iii) with a further increase in substrate temperature the atomic mobility at the surface is sufficient to allow the full atomic rearrangements necessary for the formation of equilibrium phases. By relating the distance an atom can move on the surface during deposition to substrate temperature and deposition rate, it has proved possible to account for the temperature ranges of the above deposition regimes. A hypothesis is put forward that relates the non-equilibrium phases formed in the first kinetic regime to free energy against composition diagrams at the temperature of the substrate, and this provides the basis for understanding the complex non-equilibrium phase formation found in the Cu–Sn system.

1. Introduction

The use of thin films in equilibrium phase diagram studies holds great promise in that by using the correct deposition geometry, an alloy film can be co-deposited containing concentration gradients which mimic those in both binary or ternary isothermal sections of phase diagrams [1–3]. The ability to generate an isothermal section in this way, containing all the equilibrium phases, could dramatically reduce the time taken to study alloy systems. This is of particular relevance to ternary alloys. Work done in 1965 on Fe–Ni–Cr alloys showed that thin films of this type, deposited on to substrates at the temperature of interest, produced very reasonable representations of the phase equilibria in the isothermal sections [1]. However, since then no equilibrium phase diagram studies utilizing a similar experimental technique have been reported. The most substantial obstacle to using this experimental technique is that non-equilibrium phases are readily formed during co-deposition [4], and it is therefore necessary to be able to predict the conditions under which alloy films can be deposited with equilibrium structures.

Alloys of Cu–Ag and Pd–Rh were initially examined as both are simple alloy systems containing two FCC phases and essentially deposit in a similar fashion containing similar structures. From the results of these films, a theory of phase formation was constructed based on a diffusional breakdown of initially homogeneous depositing atoms on the surface of the film during deposition. This model has enabled a good understanding of non-equilibrium phase formation to be developed [5], and from this standpoint the complex behaviour of Cu–Sn alloys was analysed. The deposition conditions for equilibrium phase formation in Cu–Sn were assessed, and films containing composition gradients and equilibrium phases deposited.

2. Experimental method

The films were produced by secondary ion beam deposition, which proved to be a very flexible and satisfactory method. The ion beam sources used were B11W fine beam saddle-field ion sources manufactured by Ion Tech Ltd., (Teddington, Middlesex.) These operate by cold-cathode discharge at low chamber pressures ($< 10^{-4}$ mbar or 10 mPa) without a magnetic field, and use 99.999% pure argon. A 1.5 mm diameter ion beam is produced, this dimension being controlled by the internal electrode structure [6, 7]. As the source field is symmetrical about the anode plane, two beams are excited, one of which can be used to continually monitor the source during deposition.

Three deposition geometries were used in this work and produced films containing either single uniform compositions, or films containing concentration gradients that mimic a binary isothermal phase diagram section. The first geometry is obtained by simply sputtering an alloy target so that a uniform composition is deposited. This is satisfactory when the target contains a single-phase structure. After an initial sputtering time, when preferential sputtering produces a surface layer rich in one atomic species, a steady state is reached, and the composition of the

0022–2461/87 $03.00 + .12

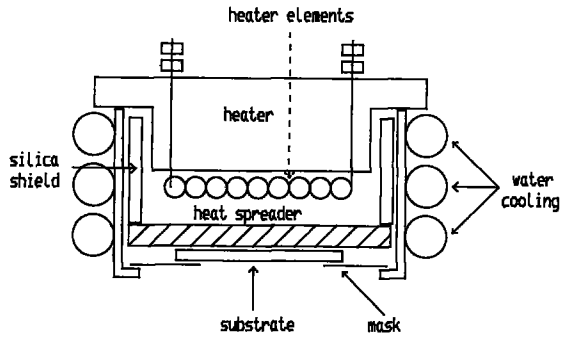

Figure 1 Schematic representation of the substrate heater and holder.

sputtered atoms becomes the same as that of the target [8].

If the target contains a two-phase structure, it is possible that variable results might be obtained because the surface-area fraction of the two phases can change as the surface is eroded. In these circumstances targets of Element A and Element B can be placed next to each other and the substrate directly within the central region of the plume of both sputtered targets. From knowledge of the deposition rate of each element and manipulation of the ion-beam currents, a uniform film of the desired composition can be produced. If a concentration gradient is required this is achieved by separating the targets and utilizing the near-cosine deposition geometry of sputtered films [9] after the fashion of Adams *et al.* [2].

Deposition rates using the B11W guns are slow in comparison to those found in processes such as planar magnetron sputtering, for example; a typical rate was $\sim 50\,\text{nm}\,\text{hr}^{-1}$. However, for equilibrium phase formation it will be shown later that slow deposition rates can be desirable. The sources require time to thermally equilibriate and during this stabilizing period the substrate is protected by a shutter. This also allows the target(s) to be sputter-cleaned before deposition. Typical chamber pressures during deposition were 10^{-4} to 10^{-5} mbar (10 to 1 mPa).

The substrate temperature was controlled by a small heating source placed within a water-cooled substrate holder. The holder and heater are shown schematically in Fig. 1. The heater is held at a fixed distance from a Nichrome heat spreader to produce an even temperature profile over the sample. Although with this experimental configuration it was not possible to directly measure the temperature of the substrate during deposition, the heater was calibrated by putting a Nichrome plate (of the same dimensions as the heat spreader) with a thermocouple attached, in place of the heat spreader and substrate. By monitoring the current and temperature at various transformer voltages, a calibration curve was plotted during both heating and cooling sequences, and there was almost exact correlation when these sequences were compared.

The films, typically 700 to 1000 nm thick, were examined by X-ray diffraction. Depending on the phases present in the film either a Philips 1010 X-ray diffractometer or a Debye–Scherrer camera was used. The diffractometer proved most valuable for peaks of reasonable intensity or when overlapping peaks were present. For faint lines, such as those found in some ordered phases, glancing-angle diffractometry proved an extremely useful technique.

Glancing-angle work was performed in the Debye–Scherrer camera, where the sample was placed at a glancing angle in the path of the X-rays. An X-ray sensitive film was then placed around the circumference of the camera and the sample exposed to the X-rays for 1 to 2 h. The angle of the diffracted lines in more normal powder work is measured directly from the film as the $\theta = 0$ line is readily found from the diffraction pattern [10]. However, in the glancing-angle work the silica substrate obscures half of the reflections and the $\theta = 0$ position must be measured indirectly. This can be done by measuring the angle of the strongest line in the diffractometer and using this to calibrate the film. Utilising the Debye–Scherrer camera in this way does distort its geometry as it is extremely difficult to place the portion of the film exposed to the X-rays in the exact centre of the camera. This introduces a systematic error to the measurement of the lines which is at a maximum at $2\theta = 90°$ and zero at 0 and 180°, but this can be minimized by careful positioning of the film and did not prove to be a critical factor in phase identification.

3. Results and discussion

3.1. Copper–silver and palladium–rhodium alloys

The Cu–Ag and Pd–Rh systems both exhibit miscibility gaps in the solid phase between two FCC phases (Figs 2 and 3) [11, 12]. The top of the miscibility gap is below the liquidus for Pd–Rh, whereas for Cu–Ag the gap lies well above the liquidus and a eutectic is therefore found. The films were deposited over a range of substrate temperatures, with fixed compositions, using elemental targets as described in Section 2. The composition of the Cu–Ag films was $43(\pm 2)$ at % Ag and that of the Pd–Rh films $42(\pm 2)$ at % Rh. The only detectable impurities were Al < 0.5 at % and Ar < 0.5 at %.

The films were examined using the Philips 1010 X-ray diffractometer and the results are shown in Table I. Supersaturated and equilibrium two-phase structures were observed in both alloys, but single-phase deposition was achieved only in Pd–Rh. Figs 4 and 5 show the diffraction patterns characteristic of these structures. In the Cu–Ag films, the increase in

TABLE I Structures observed in Cu–43 at % Ag and Pd–42 at % Rh alloy films

Alloy	Substrate temperature (°C)	Observed structures from X-ray diffraction
Cu–Ag	25	Non-equilibrium two-phase
	100	Non-equilibrium two-phase
	130	Non-equilibrium two-phase*
	200	Equilibrium two-phase
	300	Equilibrium two-phase
Pd–Rh	450	Single-phase
	560	Single-phase
	680	Non-equilibrium two-phase
	750	Non-equilibrium two-phase
	800	Equilibrium two-phase

*Very close to equilibrium deposition.

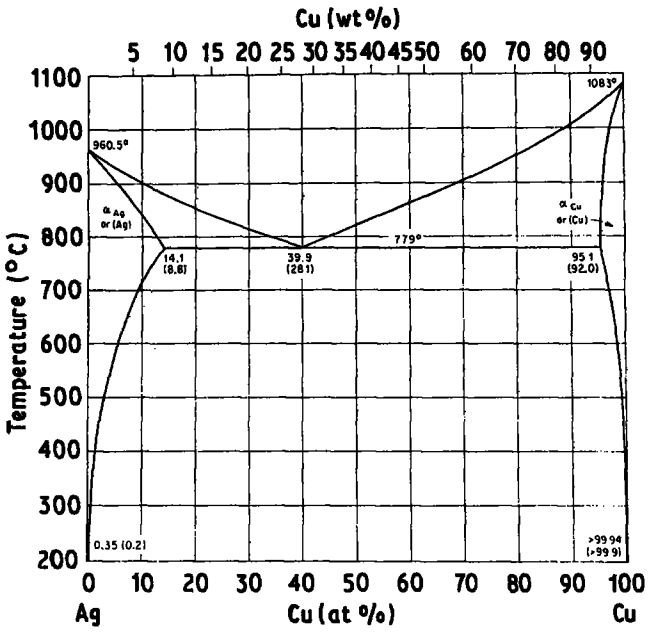

Figure 2 The Cu–Ag phase diagram [11].

the amount of supersaturation with decreasing substrate temperature indicates that single-phase deposition should occur at a temperature somewhere below 0° C and it is, therefore, reasonable to assume that a common deposition sequence with increasing substrate temperature occurs for both alloy systems: single-phase → supersaturated two-phase → equilibrium two-phase.

From this sequence it must be considered likely that kinetic conditions during deposition are the controlling factor in phase formation. Cantor and Cahn [13] suggested that ordering in aluminium alloy films was controlled by the distance an atom could move on the surface after initially depositing as a random homogeneous mixture. This distance X was limited by surface diffusion during deposition and could be expressed by the relationship

$$X \sim \left(2v\frac{a}{r_D}\right)^{1/2} a \exp\left(\frac{-Q_s}{2RT_s}\right) \quad (1)$$

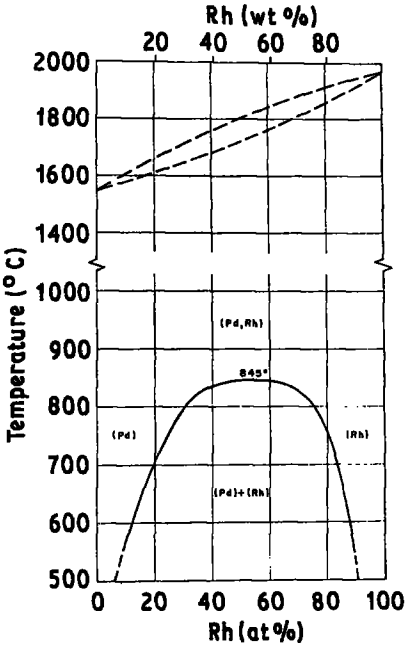

Figure 3 The Pd–Rh phase diagram [12].

where v = atomic vibrational frequency, a = atomic spacing, r_D = deposition rate, Q_s = activation energy for surface diffusion, R = gas constant and T_s = substrate temperature.

If this is extrapolated to phase formation in the Cu–Ag and Pd–Rh films, at low temperatures X will be very small and atoms that are fully intermixed in the vapour will deposit as single-phase structures. However, with increasing substrate temperature X will become sufficiently large for small atomic movements to occur on the surface, and the atoms should be able to rearrange themselves sufficiently to form supersaturated two-phase structures. At even higher temperatures X should be large enough so that the full atomic rearrangements necessary for equilibrium

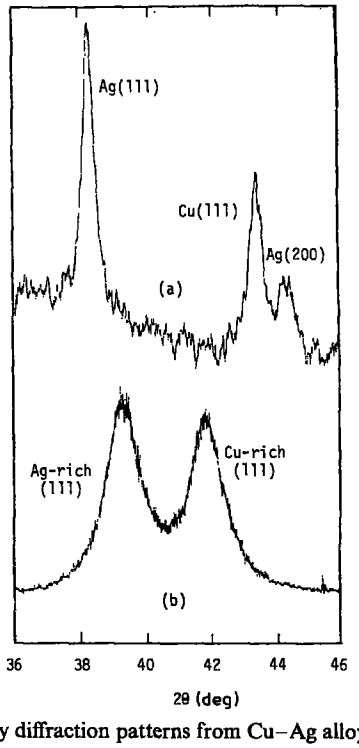

Figure 4 X-ray diffraction patterns from Cu–Ag alloy films, showing the (1 1 1) peaks of the copper-rich and silver-rich phases present: (a) deposited at 200° C showing equilibrium solubility of the phases, (b) deposited at 25° C showing supersaturation of both phases.

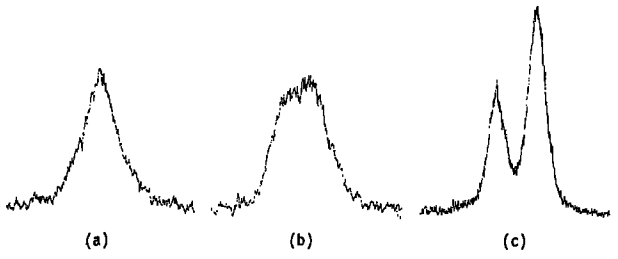

Figure 5 X-ray diffraction patterns showing the (1 1 1) peak(s) from Pd–Rh films: (a) deposited at 560° C showing a single-phase structure, (b) deposited at 750° C showing a supersaturated two-phase structure, (c) deposited at 800° C showing an equilibrium two-phase structure.

phase formation can take place. If this process occurs at the surface during deposition, plots of X against substrate temperature should show a reasonable correlation when the two binary systems are compared. However, before this is done it is necessary to consider the role of bulk diffusion in the breakdown of the depositing atoms.

Cantor and Cahn's work was performed at temperatures of less than 100 K where bulk diffusion could be ignored, hence the time a depositing atom remained on the surface of the film before being covered and enveloped in the bulk of the film was taken as a/r_D. But at high substrate temperatures the role of bulk diffusion will become significant. Atoms that are initially "buried" by the depositing atoms will be able to move back to the surface and participate again in the diffusional breakdown of the initial homogeneous mixture.

This can occur when the distance a recently deposited atom can move due to bulk diffusion is greater than the thickness of the film covering it. This is a dynamic process and therefore likely to be very complex. However, by assuming that an atom will be able to participate in the diffusional breakdown at the surface for as long as it is able to resurface, i.e. if $(D_B t)^{1/2} \geqslant r_D t$ (where D_B = bulk diffusion coefficient and t = time since depositing), a simple approximation for the additional time an atom can spend on the surface (t^*) can be derived as D_B/r_D^2, and some effect of bulk diffusion taken into account. A further modification of Equation 1 is also necessary to consider explicitly

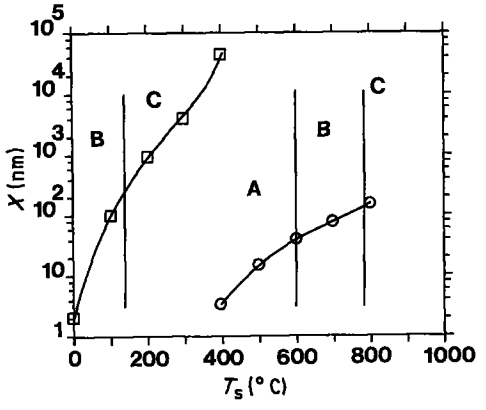

Figure 6 X against T_s plots for Cu–Ag and Pd–Rh calculated using Equation 2: (□) Cu–Ag, (○) Pd–Rh. Deposition regimes are indicated as A = single-phase, B = non-equilibrium two-phase and C = equilibrium two-phase.

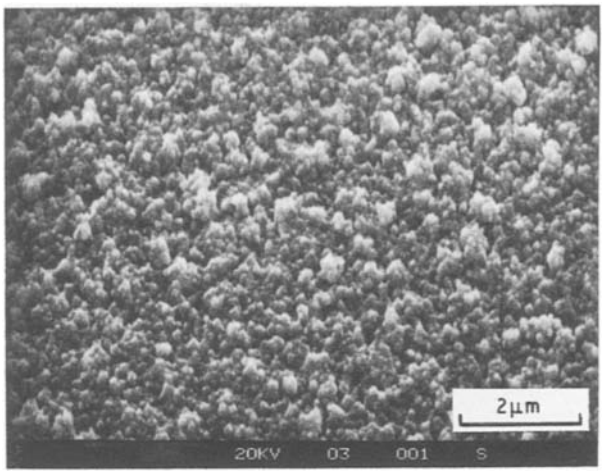

Figure 7 Scanning electron micrograph of a Cu–Ag film deposited at 200° C.

directed flow down the free-energy gradient associated with the breakdown of a single phase to a two-phase mixture. This is important in systems such as Pd–Rh where, as the top of the miscibility gap is approached, driving forces for the separation into a two-phase structure become very small. Taking the above effects into account leads to the following equation:

$$X \sim \left[2v\left(\frac{a}{r_D} + \frac{D_B}{r_D^2}\right)\right]^{1/2} a \exp\left(\frac{-Q_s}{2RT_s}\right)\left(\frac{G_T}{RT_s}\right)^{1/2} \quad (2)$$

where G_T = integral free-energy change on the formation of the equilibrium structure from the initial single phase mixture, and $D_B = D_0 \exp(-Q_B/RT_s)$, where D_0 is a constant and Q_B the activation energy for diffusion in the bulk. The diffusion constants for these systems have been assessed [14–16] and for Cu–Ag are taken as $Q_s = 71.1\,\text{kJ mol}^{-1}$, $Q_B = 188.3\,\text{kJ mol}^{-1}$ and $D_0 = 0.2 \times 10^{-4}\,\text{m}^2\,\text{sec}^{-1}$, and for Pd–Rh $Q_s = 155\,\text{kJ mol}^{-1}$, $Q_B = 314\,\text{kJ mol}^{-1}$ and $D_0 = 0.5 \times 10^{-4}\,\text{m}^2\,\text{sec}^{-1}$. G_T values were obtained from a sub-regular solution analysis of Cu–Ag and Pd–Rh.

Fig. 6 shows X against T_s plots calculated using Equation 2. From extrapolation of the supersaturation of the non-equilibrium two-phase structures in Cu–Ag, the single-phase → non-equilibrium two-phase transition is expected to occur between −20 and −40° C. This temperature is associated with a calculated X of ~0.5 nm, of the order of an atomic spacing as might be reasonably anticipated from the proposed model. The non-equilibrium two-phase → equilibrium transition in the same system occurs at a calculated X of ~300 nm. Fig. 7 shows a scanning electron micrograph of the film deposited at 200° C, which contains copper-rich and silver-rich grains that have spherodized. As X for the formation of the equilibrium two-phase structure would be expected to be of the order of the grain size, the comparison is again very good.

Fig. 8 shows the surface of the Pd–Rh film deposited at 800° C, and two features are apparent: a background of palladium-rich grains with numerous rhodium-rich precipitates on the surface. As the interprecipitate spacing is ~500 nm a predicted value for X of 150 nm is very reasonable. The X value for the

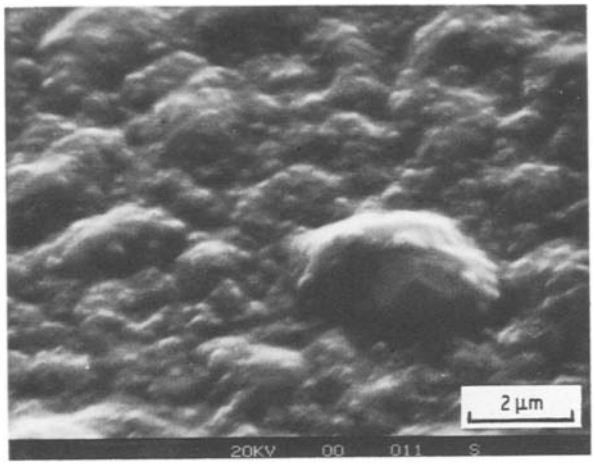

Figure 8 Scanning electron micrograph of a Pd–Rh film deposited at 800° C.

single phase → non-equilibrium two-phase transition is, however, high. Although the composition of both the Cu–Ag and Pd–Rh films place them within the spinodal of their respective systems, it is clear that a nucleation and growth process is occurring in both alloys [16]. Analysis of possible strain-energy terms for the nucleation of a second phase on the surface of a Pd–Rh film show that in comparison to Cu–Ag this system would be particularly sensitive to such a term, and this may provide a possible explanation for a large value of X.

The proposed model correctly predicts the experimentally observed deposition sequence with increasing substrate temperature, which is single-phase → non-equilibrium two-phase → equilibrium two-phase. The X against T_s plots, for the most part, account satisfactorily for the temperature ranges of the deposition regimes, although the proper incorporation of a strain-energy factor is desirable for future work in systems where coherent interfaces can occur. The next section presents an analysis of the results observed in the much more complex system, Cu–Sn.

3.2. Copper–tin alloys

The Cu–Sn system (Fig. 9) has been studied extensively and no major changes have been reported since the review of Hansen and Anderko [11]. There are two terminal solid solutions, the Cu(fcc) and Tin(bct) phases, and six intermediate phases which are listed below [17]:

(i) The β phase with an A2 structure.
(ii) The γ phase, ordered with a DO3 structure.
(iii) The δ phase, cubic with an ordered gamma brass structure (a = 1.799 nm).
(iv) The ζ phase, an ordered hexagonal structure based on the AgZn ζ unit cell.
(v) The ε phase that has been described by a number of superlattices based on an ordering of an A3 cph unit cell.
(vi) The η phase, an ordered hexagonal structure, based on the B81 NiAs unit cell.

Two alloys of 11.5 at % Sn and 19.5 at % Sn were deposited on to silica substrates, over a range of substrate temperatures, by sputtering of single-phase Cu–Sn alloy bulk targets. The composition of the films differed from that of the alloy targets, being copper-rich. This is probably due to selective resputtering

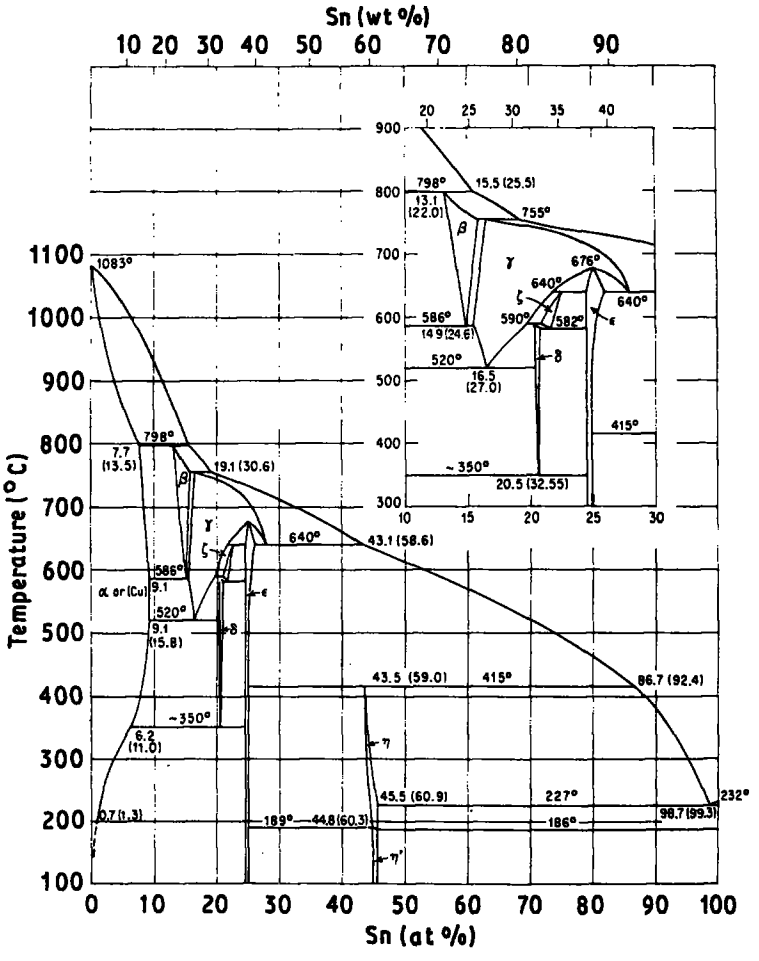

Figure 9 The Cu–Sn phase diagram [11].

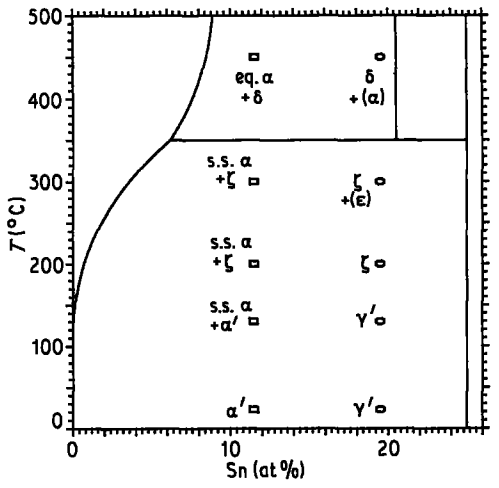

Figure 10 Summary of X-ray diffraction results from the Cu–Sn films: s.s. = supersaturated, eq. = equilibrium. Phases in brackets indicate very few lines available for identification from X-ray diffraction.

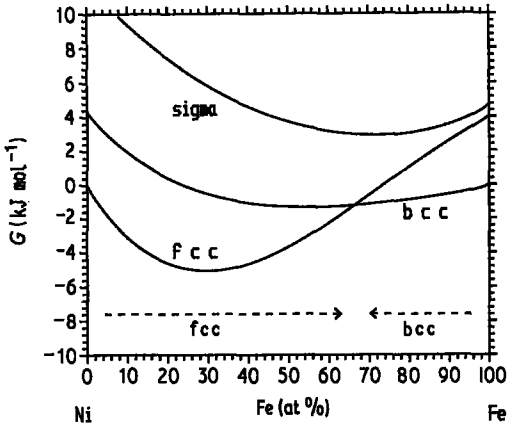

Figure 11 G–x diagram for Ni–Fe at 100° C [19], with the reported microstructures from alloy films codeposited on to substrates at 100° C [18]; (←– – –→) reported supersaturation.

[18] which occurs when there are differences in sputter yield of the alloy components. This leads to the higher yield component being preferentially removed from the growing film due to resputtering. This is consistent with the sputter rate of tin found in this study being greater than that of copper. The films, although different in composition from the target, deposited with consistent copper/tin ratios and the compositions quoted are accurate to within 0.5 at %.

The films were deposited over a temperature range of 25 to 450° C. At 450° C both alloys deposited with equilibrium phases. At lower substrate temperatures the films were characterized by the formation of the ζ phase between 200 and 300° C, and below 200° C by two phases which are not observed in the phase diagram. These are described below:

1. The α' phase. The measured d spacings from glacing-angle X-ray diffraction can be categorized by a cph A3 lattice, where $a = 0.2625$ nm and $c = 0.426$ nm; $c/a = 1.623$. The occurrence of such a phase in other copper binaries with Group IVb and Vb elements is quite common: Cu–Si, Cu–Ge and Cu–Sb all contain stable cph phases at similar electron/atom ratios.

2. The γ' phase. The structure of this phase is a γ-brass type, with a cubic cell $a = 0.899$ nm. It is therefore closely related to the equilibrium delta phase, which is formed by a further ordering of the γ-brass structure so that a is doubled to 1.799 nm.

The results are summarized in Fig. 10. A similar sequence of phase formation is observed in the Cu–Sn films as in the Cu–Ag and Pd–Rh films, i.e. single-phase → non-equilibrium two-phase → equilibrium phase(s). However, the Cu–Sn system contains a number of different phases and, as might be expected, the formation of non-equilibrium phases is more complex. The present authors [5, 16] have proposed a hypothesis for predicting non-equilibrium phase formation in co-deposited alloy films, which can be summarized in the following way.

Depositing atoms lose their kinetic energy within a few atomic vibrations [19] and any transformation involving an intermediate high temperature phase, whether it be a liquid or solid phase, must be considered highly unlikely. Nucleation and growth processes are controlled by the substrate temperature [4] and, therefore, when X is less than a few atomic spacings, the structure of the film should reflect the most energetically stable single-phase structure available to it at the temperature of the substrate. This phase can be found directly from the free energy (G) against composition (x) diagrams of the alloy system of interest.

The authors have analysed a number of systems where both co-deposition and thermodynamic analysis have been reported, and the correlation between the structures observed and G–x diagrams is very good [5, 16]. This can be demonstrated for the Ni–Fe system. Fig. 11 shows the G–x diagram of Ni–Fe at 100° C [20] with the structures observed in films co-deposited at that temperature [21]. By using heats of crystallization in conjunction with phase diagram calculations [5, 22, 23], the model has been shown to be applicable for amorphous phase formation.

X against T_s plots for both the 11.5 and 19.5% alloys have been evaluated previously [16] and these are shown in Fig. 12. Good agreement with experiment is found with a prediction for the deposition regimes based on $X = 5$ nm for the single phase → non-equilibrium two-phase transition, and 1000 nm for the formation of equilibrium structures. The authors have thermodynamically evaluated the Cu–Sn system [24] and Fig. 13 shows the G–x diagrams for Cu–Sn between 25 and 300° C in the composition range of interest.

In the 11.5 at % Sn alloy the α' phase is formed in the single-phase regime in agreement with the G–x diagram. Although a disordered cph phase is not observed in the Cu–Sn equilibrium phase diagram, the free energy of such a phase can be estimated from stacking fault energies [25] and included in the thermodynamic evaluation. In the non-equilibrium two-phase region the films adopt a metastable equilibrium between supersaturated α and the α'/ζ phases, which is energetically favourable as an intermediate step before complete equilibrium is reached.

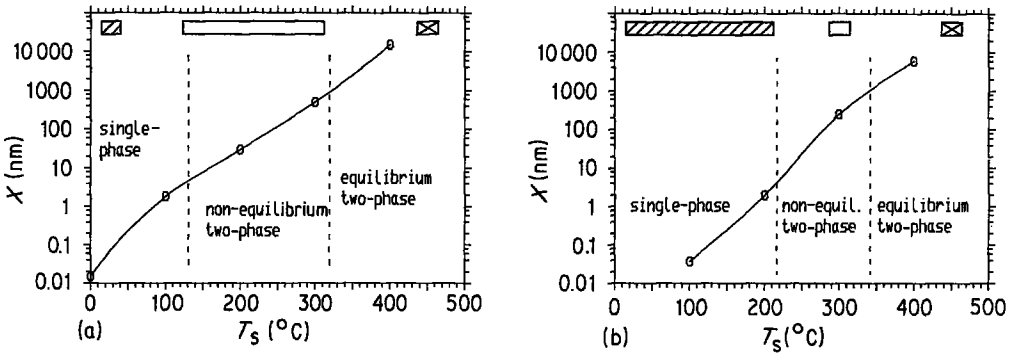

Figure 12 X against T_s plots for (a) Cu–11.5 at % Sn and (b) Cu–19.5 at % Sn films [16], showing deposition regimes based on $X = 5$ nm for the single-phase → non-equilibrium two-phase transition and $X = 1000$ nm for equilibrium phase formation. Experimental results are shown in the top of the diagrams: ▨ single-phase, □ non-equilibrium two-phase, ⊠ equilibrium two-phase.

The ζ phase is formed in the 19.5 at % Sn alloy as would be predicted. However, at 25 and 130° C the ζ' phase is preferred. This effect cannot be assessed from thermodynamic considerations as insufficient phase stability data are available for this phase. A number of aspects concerning the formation of complex ordered structures remain to be clarified. For example, in the Ni–Cr system while σ-phase formation is predicted [5] and observed between ~50 to 84 at % Cr [26, 27], various other ordered phases are also seen at similar compositions [26, 28, 29]. It may be that differences in surface mobility can stabilize different ordered structures, which might suggest that there is little difference in free energy between them. This would be consistent for the 19.5 at % Sn alloy, as the ζ phase is closely related to a γ-brass structure [30].

Overall phase formation in the Cu–Sn films appears to be explained very satisfactorily. The single phase → non-equilibrium two-phase → equilibrium phase(s) sequence is accounted for very well, and although in the 19.5 at % films the γ' phase is formed in preference to the ζ phase at room temperature and 130° C, the formation of the ζ and α' phases is clearly predicted.

Following these experiments, Cu–Sn films were deposited containing composition gradients (see Section 2) to confirm that equilibrium phase formation would be observed in such films. Two substrate temperatures of 400 and 500° C were used. At both of these temperatures the equilibrium phases were formed, and Fig. 14 shows the diffraction patterns obtained from the film deposited at 500° C. The transitions from $\alpha \rightarrow \alpha + \delta \rightarrow \delta \rightarrow \delta + \varepsilon \rightarrow \varepsilon$ are clearly distinguishable, and calculation of lattice parameters shows that the composition of the phases is that predicted by the phase diagram [17].

4. General discussion

The model for phase formation put forward here

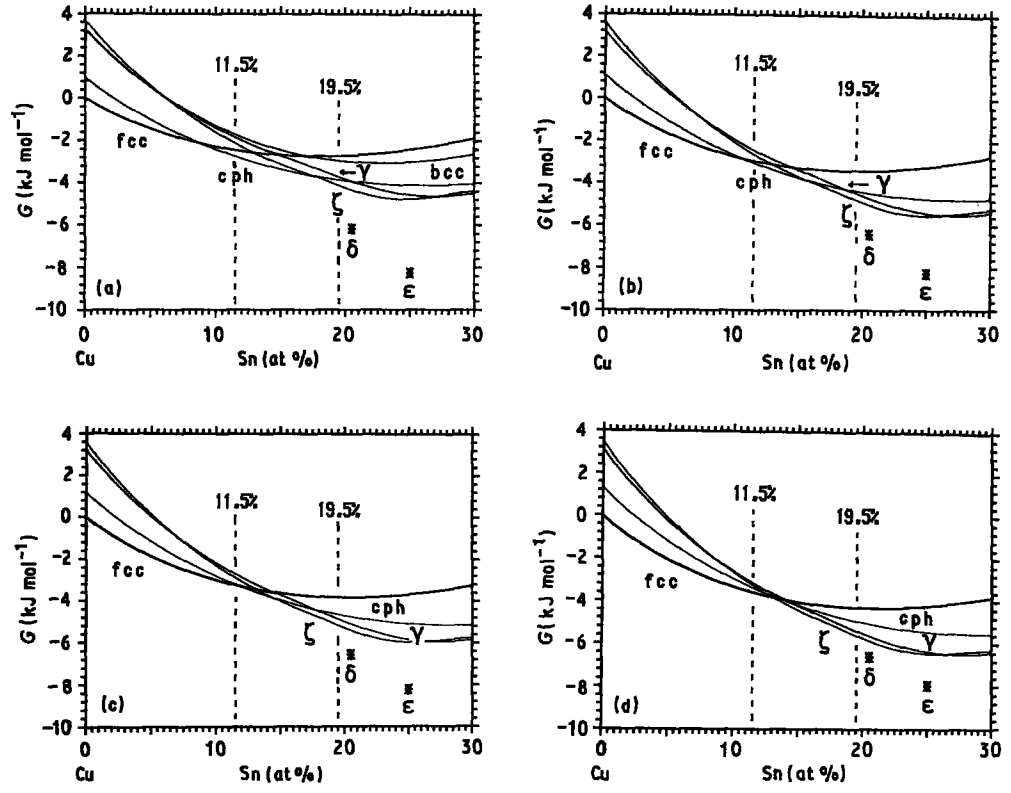

Figure 13 G–x diagrams for Cu–Sn (0 to 30 at % Sn) at (a) 25° C (b) 130° C (c) 200° C and (d) 300° C.

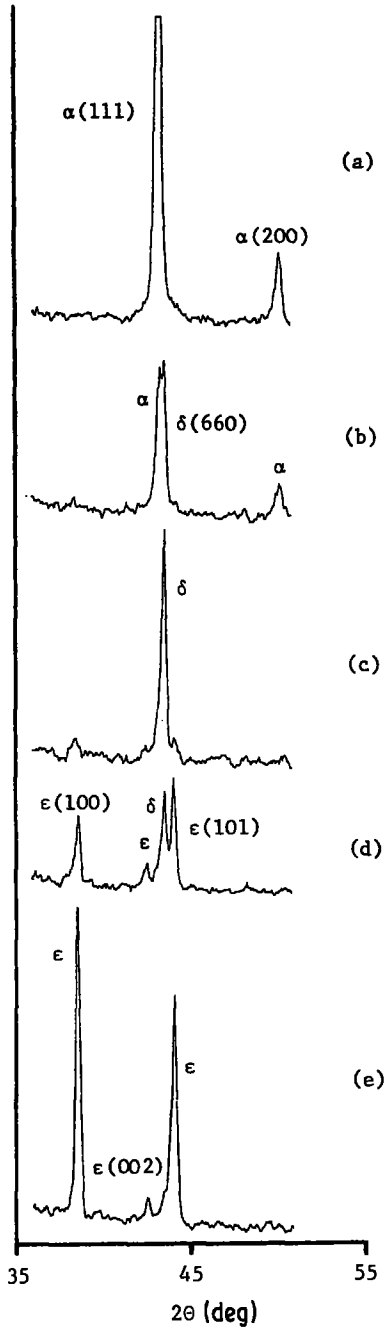

Figure 14 X-ray diffraction patterns from a gradient-deposited Cu–Sn film showing (a) the α phase, (b) the α + δ phases, (c) the δ phase (with a small amount of ε), (d) the δ + ε phases, (e) the ε phase.

explains the experimentally observed deposition regimes extremely well, and is confirmed by studies of other systems such as Al–Ni [13, 31], Al–Ag [2] and Fe–Ni–Cr [20], where similar sequences of phase formation with substrate temperature are observed. However, the factors controlling the formation of non-equilibrium ordered phases are not clearly defined by this work or by other studies. For example although Cantor and Cahn [13] suppressed ordering in Al–Cu and Al–Ni alloys by depositing at liquid nitrogen temperatures, they were unable to achieve this in Al–Fe alloys at similar temperatures. The formation of the γ′ phase in preference to the ζ phase at 130° C and below has already been mentioned. There are a number of conceptual difficulties in modelling non-equilibrium ordered phase formation in co-deposited thin films as, in the main part, the principles that underly the relative stability of many of these structures are not at all clearly understood. Future work may then be forced to rely on qualitative, empirical rules, until the understanding of the stability of these phases becomes clearer.

The possible effect on phase formation of process variables, such as gas pressure or different deposition techniques, has not been considered. These roles are difficult to quantify and can be very specific to particular deposition techniques. For example, glow-discharge deposition is not usually performed at the vacuums achieved by secondary ion beam deposition, and the uptake of the ionizing gas might therefore be expected to be greater. Although chemically inert, gases such as argon (commonly used in sputter deposition) may be able to adopt substitutional sites in some metals [32], and the ensuing distortions then placed on the crystal structure could affect phase stability quite significantly. Other effects such as the adsorption of impurities on to the surface of the film during deposition may under certain conditions become important [4]. The most potent impurities appear to be the light elements such as nitrogen and oxygen [4, 33], which are also powerful modifiers of thermodynamic stability. The modelling of phase formation therefore relies to a large extent on a good vacuum being maintained, the sputter gas being chemically inert, and the uptake of ionizing gas and impurities, particularly light elements, being small.

The capability of the model put forward here to predict the deposition conditions for equilibrium phase formation is dependent to a large extent on some knowledge of the diffusion coefficients. In many systems these are not known or there is some scatter in the experimentally observed coefficients. However, one of the features of this study has been the rapid achievement of equilibrium in the films. For example, the confirmation of a miscibility gap in Pd–Rh by the formation of a two-phase structure at 680° C is an improvement of orders of magnitude on the time taken to obtain this in bulk samples. In these terms the achievement of equilibrium at 200° C in the Cu–Ag films is also quite remarkable and it should, therefore, be possible to ensure that equilibrium deposition is achieved by depositing well above the predicted substrate temperature. Another and more preferable alternative is to deposit over a range of substrate temperatures which includes both single-phase and equilibrium deposition. The sequence of phase formation can then be more clearly resolved, with the added advantage that any thermodynamic modelling can to some extent be checked by comparison with the phases observed in the first kinetic regime.

5. Conclusions

1. The major factor in multiphase formation in co-deposited alloy thin films is the diffusional breakdown of fully intermixed depositing atoms during deposition.

2. Three kinetic regimes are observed as the substrate temperature is varied. At low substrate temperatures the surface mobility is insufficient for the

decomposition of the fully intermixed depositing atoms, and the films are constrained to be single-phase. With increasing substrate temperature, decomposition to a non-equilibrium two-phase structure is observed. Finally, with a further increase in substrate temperature the atomic mobility becomes sufficient to allow the full atomic rearrangements necessary for the formation of equilibrium phases.

3. By relating the distance an atom can move on the surface of the film during deposition with substrate temperature and deposition rate, the transition to equilibrium phase formation can be accurately accounted for in all the films studied.

4. Equilibrium phase formation can be achieved extremely rapidly in co-deposited alloy thin films.

5. The complex deposition behaviour of the Cu–Sn alloys can be explained very satisfactorily by using a hypothesis that relates the phases formed at low substrate temperatures to free energy against composition diagrams at the temperature of the substrate.

Acknowledgements

The authors gratefully acknowledge the financial support of the Science and Engineering Research Council.

References

1. K. KENNEDY, T. STEFANSKY, G. DAVEY, V. ZACKAY and E. PARKER, *J. Appl. Phys.* **32** (1965) 3808.
2. R. O. ADAMS, C. W. NORDIN and K. D. MASTERSON, *Thin Solid Films* **72** (1980) 335.
3. T. W. BARBEE and D. L. KEITH, in "Synthesis and Properties of Metastable Phases", edited by E. S. Machlin and T. J. Rowland (MSA Alloy Phases Committee, Pittsburgh, 1980) p. 93.
4. K. L. CHOPRA, "Thin Film Phenomena" (McGraw-Hill, New York, 1969).
5. N. SAUNDERS and A. P. MIODOWNIK, *CALPHAD* **9** (1985) 283.
6. A. M. GHANDER and R. FITCH, *Vacuum* **24** (1974) 483.
7. J. FRANKS and A. M. GHANDER, *ibid.* **24** (1974) 489.
8. M. H. FRANCOMBE, in "Epitaxial Growth", edited by J. W. Matthews (Academic Press, New York, 1975) p. 109.
9. W. SCAIFE, P. HANLEY and K. PURSER, in Proceedings of 4th International Conference of the Nuclear Target Development Society, Argonne, 1975, p. 74.
10. B. D. CULLITY, "Elements of X-ray Diffraction" (Addison-Wesley, New York, 1967).
11. M. HANSEN and K. ANDERKO, "Constitution of Binary Alloys" (McGraw-Hill, New York, 1958).
12. R. P. ELLIOTT, "Constitution of Binary Alloys; First Supplement" (McGraw-Hill, New York, 1965).
13. B. CANTOR and R. W. CAHN, *Acta Metall.* **24**, (1976), 845.
14. D. BUTRYMOWICZ, J. MANNING and M. READ, *J. Phys. Chem. Ref. Data* **3** (1974) 527.
15. J. ASKILL, in "Tracer Diffusion Data for Alloys and Simple Oxides" (Plenum Press, New York, 1970).
16. N. SAUNDERS, PhD thesis, University of Surrey (1984).
17. W. B. PEARSON, "Handbook of Lattice Spacings and Structures of Metals and Alloys" (Pergamon Press, London, 1958).
18. L. I. MAISSEL, in "Handbook of Thin Film Technology", edited by L. I. Maissel and R. Glang (McGraw-Hill, New York, 1970) p. 4.
19. J. LENNARD-JONES, *Proc. R. Soc.* **A163** (1963) 127.
20. T. G. CHART, F. PUTLAND and A. DINSDALE, *CALPHAD* **4** (1980) 27.
21. S. MUKHERJEE and B. ROGALLA, *Thin Solid Films* **56** (1979) 279.
22. N. SAUNDERS and A. P. MIODOWNIK, *J. Mater. Res.* **1** (1986) 38.
23. N. SAUNDERS, *Int. J. Rapid Solidification* **1** (1985) 327.
24. A. P. MIODOWNIK, *J. Less-Common Metals* **114** (1985) 81.
25. *Idem, CALPHAD* **2** (1978) 207.
26. N. YUKAWA, M. HIDA, T. IMURA, K. KAWAMURA and Y. MIZUNO, *Met. Trans.* **3** (1972) 887.
27. H. J. SCHULLER and P. SCHWAAB, *Z. Metallkde* **51**, (1960) 81.
28. M. BIRJEGA, N. POPESCU-POGRION, C. SARBU and S. RAU, *Thin solid Films* **34** (1976) 153.
29. J. MOOIJ and M. DE JONG, *J. Vac. Sci. Tech.* **9** (1972) 446.
30. O. CARLSSON and C. HAGG, *Z. Krist.* **A83** (1932) 308.
31. T. G. HENTZELL, B. ANDERSSON and S. -E. KARLSSON, *Acta Metall.* **31** (1983) 1131.
32. C. F. MELIUS, W. D. WILSON and C. L. BISSON, *Radiat. Effects* **53** (1980) 111.
33. A. TODD, private communication (1985).

Received 3 March
and accepted 22 May 1986